AGU PUBLICATIONS

Geophysical Research Letters

RESEARCH LETTER
10.1002/2014GL060438

Key Points:
- We propose a scaling law that predicts shear zone thickness in the lithosphere
- Shear zone thickness depends on material parameters and loading conditions
- Two-dimensional numerical results support the analytical prediction

Supporting Information:
- Readme
- Figure S1

Correspondence to:
T. Duretz,
thibault.duretz@unil.ch

Citation:
Duretz, T., S. M. Schmalholz, Y. Y. Podladchikov, and D. A. Yuen (2014), Physics-controlled thickness of shear zones caused by viscous heating: Implications for crustal shear localization, *Geophys. Res. Lett.*, *41*, 4904–4911, doi:10.1002/2014GL060438.

Received 6 MAY 2014
Accepted 1 JUL 2014
Accepted article online 5 JUL 2014
Published online 21 JUL 2014

Physics-controlled thickness of shear zones caused by viscous heating: Implications for crustal shear localization

T. Duretz[1], S. M. Schmalholz[1], Y. Y. Podladchikov[1], and D. A. Yuen[2,3,4]

[1]Institut des Sciences de la Terre, Bâtiment Géopolis, Lausanne, Switzerland, [2]Minnesota Supercomputing Institute, University of Minnesota, Minneapolis, Minnesota, USA, [3]Department of Earth Sciences, University of Minnesota, Minneapolis, Minnesota, USA, [4]School of Environmental Sciences, China University of Geosciences, Wuhan, China

Abstract We evaluate the parameters that control the thickness of ductile shear zones that are generated by viscous heating. We employ two-dimensional thermomechanical numerical models to simulate shear zone development under compression. Results show that the shear zone thickness is essentially independent on the numerical resolution and the initial size of a weak inclusion that triggers shear localization. A simple scaling law is derived which predicts the thickness with six physical parameters: far-field stress and strain rate, thermal conductivity (both constant and temperature dependent), initial temperature, activation energy, and stress exponent. The scaling law is confirmed by numerical simulations for a wide range of parameters. For crustal deformation conditions typical temperature increase ranges between 50°C and 200°C, and the predicted thickness is between 1 km and 7 km. These thicknesses agree with natural crustal and lithospheric shear zones suggesting that shear heating is a process controlling crustal shear zone formation.

1. Introduction

Ductile shearing is a widespread mode of lithospheric deformation, and the occurrence of kilometer-scale shear zones at plate boundaries is a key ingredient of plate tectonics [*Gibbons*, 2008]. These shear zones represent essential features of subduction zones [*Yuen et al.*, 1978; *Cloos and Shreve*, 1996], lithospheric extension [*Davis*, 1983; *Wernicke*, 1985], and transcurrent deformation [*Yuen et al.*, 1978; *Brun and Cobbold*, 1980; *Thatcher and England*, 1998; *Leloup et al.*, 1999]. At the crustal scale, ductile shear zones are well represented in orogens [*Ramsay*, 1980] where tectonic nappes are often considered as plurikilometric ductile shear zones [*Steck*, 2008; *Steck et al.*, 2013]. At these scales, thermal weakening due to viscous heating is generally considered as an important process for the development and maintenance of shear zones [*Yuen et al.*, 1978; *Brun and Cobbold*, 1980; *Fleitout and Froidevaux*, 1980; *Regenauer-Lieb and Yuen*, 2003; *Kaus and Podladchikov*, 2006; *Braeck and Podladchikov*, 2007; *John et al.*, 2009; *Thielmann and Kaus*, 2012; *Minakov et al.*, 2013; *Schmalholz and Podladchikov*, 2013; *Walley*, 2007; *Wright*, 2002; *Dodd and Bai*, 2012; *Takeuchi and Fialko*, 2012]. Viscous heating is also considered as an important mechanism taking place during intermediate depth earthquake rupture [*Prieto et al.*, 2013]. The geodynamic interpretation of natural pressure-temperature estimates within or in the vicinity of shear zones requires a thorough understanding of their thermomechanical behavior [*Bird*, 1978; *England and Molnar*, 1993; *Duprat-Oualid et al.*, 2013]. The thickness of shear zone has indeed a strong impact on the strain rate, stress, pressure, and temperature distribution inside shear zones [*Fleitout and Froidevaux*, 1980]. However, the parameters that control the thickness of ductile shear zones within rocks are until now still not well understood. Here we employ two-dimensional (2-D) thermomechanical numerical simulations, based on the finite difference/marker-in-cell (FD/MIC) method, to model the development of shear zones due to viscous heating. The shear zones are triggered by a weak circular inclusion, and the employed rheologies are described by flow laws typical for crustal rocks. We show that the thickness of these shear zones is only controlled by the material properties and far-field loading conditions. Furthermore, we derive an approximate scaling law for the shear zone thickness which can be used to predict the shear zone thickness.

2. Mathematical Model

We consider the deformation of power law viscous incompressible fluid with thermomechanical coupling. The transient energy balance equation is hence coupled to the heat dissipated by irreversible

Table 1. Material Parameters Used in the Reference Simulations[a]

Material	A (Pa^{-n} s^{-1})	n	E_a (kJ/mol)	k (W/m/K)	$k(T)$ (W/m/K)	C_p (J/kg/K)	ρ (kg/m^3)
Matrix	3.20×10^{-20}	3.0	276	2.5	$1.72 + \frac{807}{T+350}$	1050	2700
Inclusion	3.16×10^{-26}	3.3	186	2.5	$1.72 + \frac{807}{T+350}$	1050	2700

[a]The temperature-dependent conductivity law was employed for the experiments depicted on Figure 4. The parameters were modified after *Clauser and Huenges* [1995] in order to provide a conductivity equal to the reference conductivity ($k = 2.5$ W/m/K) when the initial temperature is equal to the reference temperature ($T_0 = 400°C$).

mechanical work:

$$\rho C_p \frac{DT}{Dt} = \frac{\partial}{\partial x_i}\left(k\frac{\partial T}{\partial x_i}\right) + \dot{\epsilon}_{ij}\tau_{ji}, \tag{1}$$

where T, ρ, C_p, x_i, and k, respectively, stand for the temperature, density, specific heat capacity, spatial coordinates, and thermal conductivity (Table 1). The latter can be either constant or temperature dependent [*Clauser and Huenges*, 1995] (Table 1). The inner product of the viscous deviatoric stress (τ_{ij}) and strain rate tensors ($\dot{\epsilon}_{ij}$) represents the viscous heating source term. For steady state creep and in the absence of body forces, the momentum balance can be written as

$$\frac{\partial \tau_{ij}}{\partial x_j} - \frac{\partial P}{\partial x_i} = 0, \tag{2}$$

where P stands for the pressure (mean stress). Mass conservation is ensured by constraining the flow to be divergence free such that

$$\frac{\partial v_i}{\partial x_i} = 0, \tag{3}$$

where v corresponds to the velocity vector. The deviatoric stress tensor relates to the strain rate tensor via the constitutive relationship:

$$\tau_{ij} = 2\,\eta_{\text{eff}}\,\dot{\epsilon}_{ij}. \tag{4}$$

The viscosity (η_{eff}) follows a thermally activated power law flow law, representative for dislocation creep deformation mechanism [*Ranalli*, 1995]:

$$\eta_{\text{eff}} = \frac{2^{\frac{1-n}{n}}}{3^{\frac{1+n}{2n}}} A^{-\frac{1}{n}} \dot{\epsilon}_{\text{II}}^{\frac{1}{n}-1} \exp\left(\frac{E_a}{nRT}\right), \tag{5}$$

where A, n, and E_a are experimentally derived material parameters (Table 1) and $\dot{\epsilon}_{\text{II}}$ is the second invariant of the deviatoric strain rate tensor, which is formulated as

$$\dot{\epsilon}_{\text{II}} = \sqrt{\frac{1}{2}\dot{\epsilon}_{ij}\dot{\epsilon}_{ij}}. \tag{6}$$

2.1. Model Configuration

The configuration consists of a 70 × 40 km domain containing a half-circular inclusion with a radius of 3 km, whose center is located at the bottom middle of the domain (Figure 1a). The lower boundary is free slip (zero tangential shear stress, zero normal velocities), whereas the upper, left, and right sides satisfy a constant background strain rate $\dot{\epsilon}_{\text{BG}}$ (time-dependant normal velocity and zero tangential shear stress) of 5×10^{-14} s^{-1}. All thermal boundary conditions are zero flux which yields to upper estimates of the temperature increase due to shear heating. The background material has Maryland diabase rheology [*Carter and Tsenn*, 1987], and the inclusion has a weaker dry Westerly granite rheology [*Carter and Tsenn*, 1987] (Table 1). The initial temperature is set at 400°C which yields to a reference stress (σ_{BG}) of 980 MPa within the Maryland diabase matrix. After a few percent of bulk shortening, shear zones with naturally developed thickness develop spontaneously. A viscosity ratio of ~100 develops at the material interface; hence, no viscosity cutoff is needed.

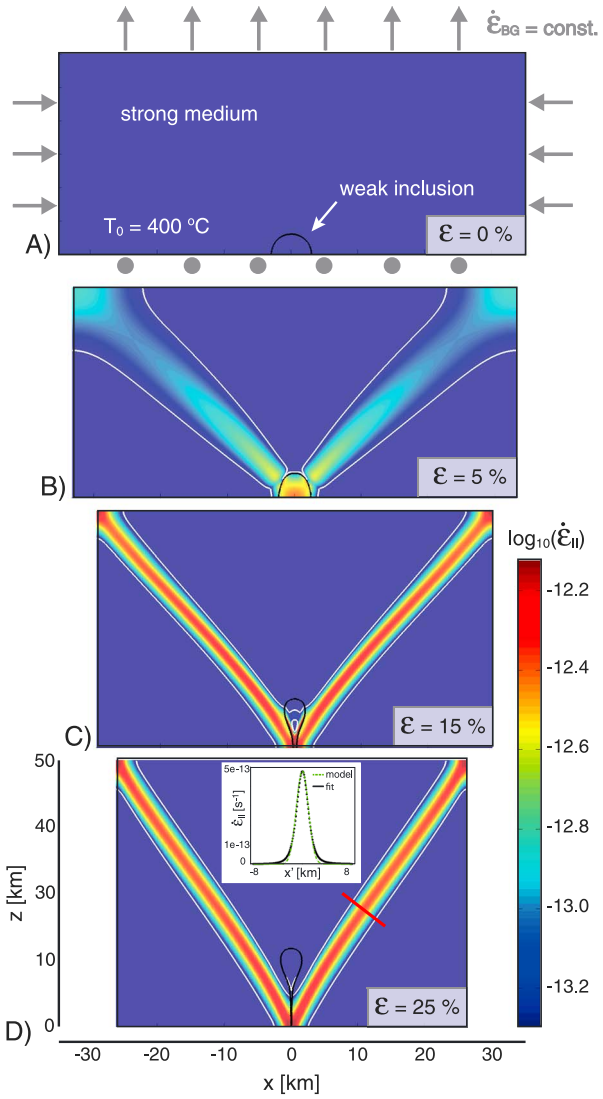

Figure 1. (a) The initial model configuration. (b–d) The model evolution until 25% bulk shortening. The color map indicates the second invariant of the strain rate tensor ($\dot{\epsilon}_{II}$). The white contours indicate model areas with higher strain rates than the background strain rate ($\dot{\epsilon}_{II} > \dot{\epsilon}_{BG}$). Black contour indicates the shape of the weak inclusion. The red line in Figure 1d corresponds to the location of evaluation of $\dot{\epsilon}_{II}$ profile.

2.2. Approximate Scaling Law

We aim at a first-order approximation of the quasi-stationary shear zone thickness. The initial temperature rise due to viscous heating is assumed to outpace the conductive cooling leading to the onset of instability and progressive shear localization (see *Kaus and Podladchikov* [2006] for the quantification of the initial temperature rise) thus justifying the use of insulating boundary condition. Based on systematic numerical simulations, we found that the thermal anomaly must be on the order of

$$\Delta T \propto \frac{T_0^3 R^2}{n^2 E_A^2} \tag{7}$$

With time, the sharpening of the thermal gradient may lead to quasi steady state balance between shear heating and conductive cooling. The time derivative in equation (1) is set to zero under quasi-static approximation; the remaining two terms balance each other:

$$k \frac{T_0^3 R^2}{n^2 E_A^2 D^2} \propto \dot{\epsilon}_{BG}\, \sigma_{BG} \tag{8}$$

The length scale, D, represents here the shear zone thickness, and this length scale appears due to the second derivative with respect to space in the diffusion term of equation (1). Solving for D yields

$$D = K \frac{R T_0}{n E_A} \sqrt{\frac{k\, T_0}{\dot{\epsilon}_{BG}\, \sigma_{BG}}}, \tag{9}$$

where K is a nondimensional constant to be determined. The above scaling law will be tested next with 2-D thermomechanical numerical simulations.

2.3. Numerical Method

We use the FD/MIC numerical method [*Gerya*, 2010]. The momentum balance and continuity equation are discretized on a staggered grid. The energy balance equation is solved implicitly using second-order backward difference formula on a cell-centered grid. Energy and material properties are transported by Lagrangian markers employing an explicit fourth-order Runge-Kutta advection scheme. The mapping between the markers and cells is carried out by one-cell interpolation [*Duretz et al.*, 2011] and arithmetic averaging. The nonlinearity inherent to the non-Newtonian rheological model is treated by using Picard iterations coupled to a line search algorithm.

2.4. Shear Zone Thickness Measurement

The thickness of the shear zone is measured using second strain rate tensor invariant ($\dot{\epsilon}_{II}$) profiles obtained in the zones of localized deformation. Within such shear zones, the stress is constant and $\dot{\epsilon}_{II}$ is therefore directly proportional to the temperature. $\dot{\epsilon}_{II}$ profiles hence follow a Gaussian distribution where the maximum $\dot{\epsilon}_{II}$

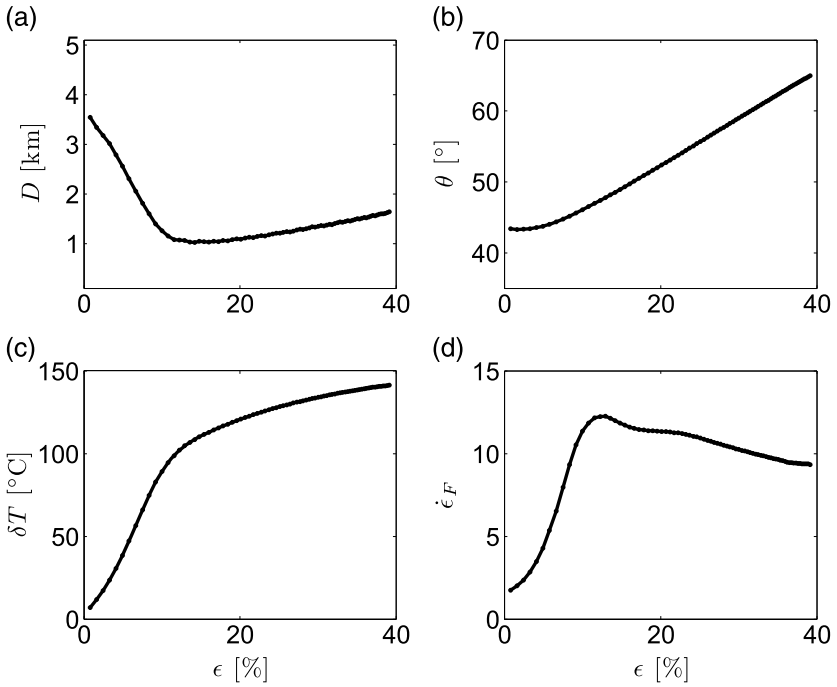

Figure 2. Transient evolution of the shear zone characteristics with progressive bulk shortening (ϵ). (a) Evolution of shear zone thickness according to criteria explained in section 2. (b) Evolution of the shear zone angle. (c) Evolution of temperature increase (δT) within the shear zone. (d) Evolution of strain rate amplification within the shear zone ($\dot{\epsilon}_F = \max \dot{\epsilon}_{II}/\dot{\epsilon}_{BG}$).

coincides with the center of the shear zone. For each numerical simulation, we define the shear zone thickness as twice the variance (2σ) of the best fitting Gaussian distribution (Figure 1d). A similar approach to determine the thickness of shear zones developing in fluid-saturated gauge material was employed by *Platt et al.* [2014].

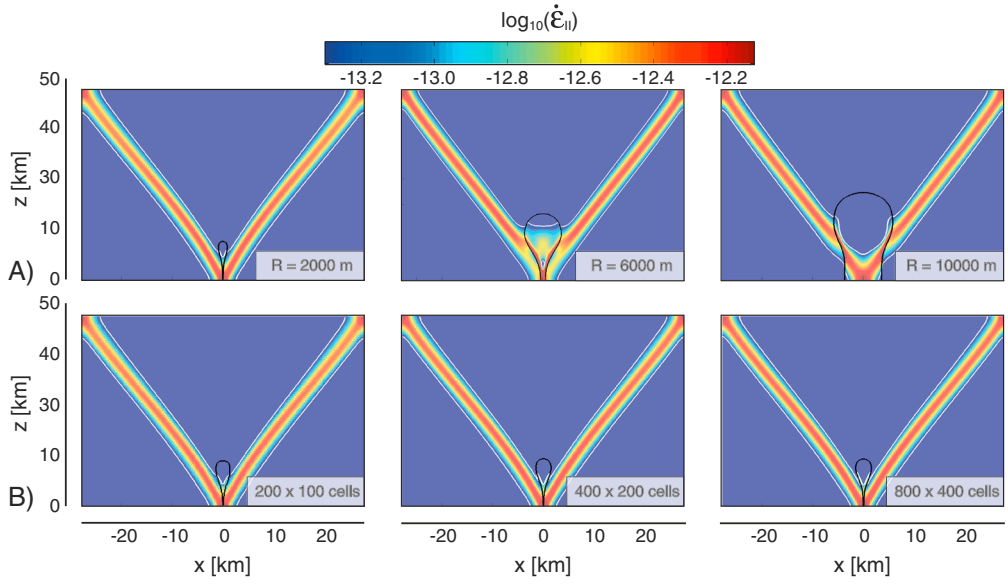

Figure 3. Shear zone after 20% shortening. (a) Results obtained for three different initial inclusion radii for the same numerical resolution (800 × 400 cells). (b) Results obtained with different numerical resolutions for the same inclusion radius (3 km). At low resolution (200 × 100 cells) less than 10 cells are needed across the shear zone. The color map and contour correspond to those used in Figure 1.

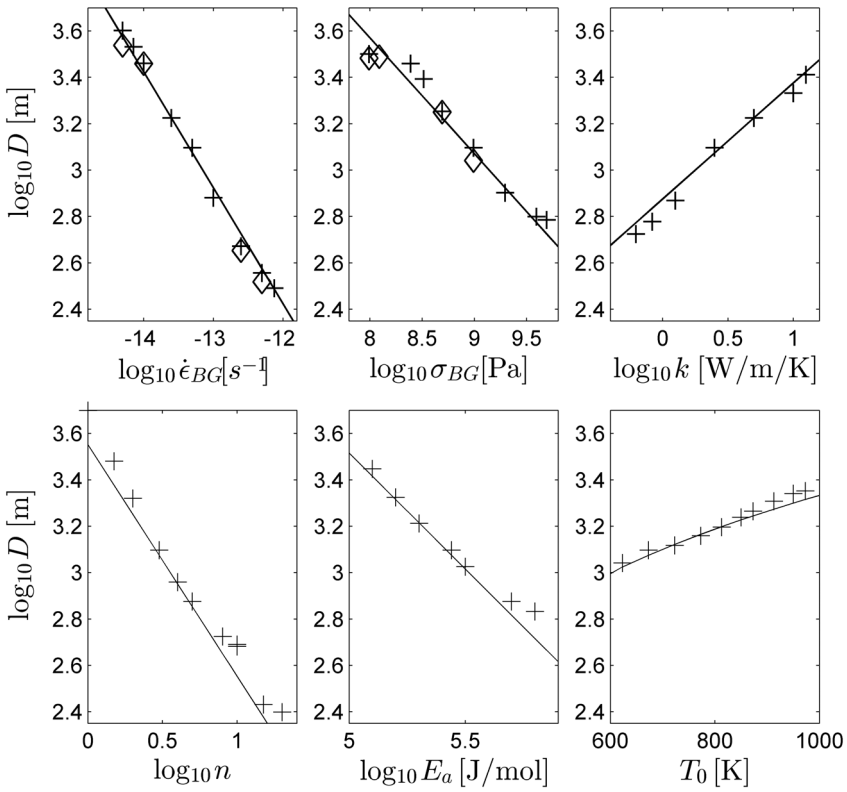

Figure 4. Dependence of the shear zone thickness (D) on the controlling physical parameters. (a) The dependence of D on the background strain rate for a constant background stress (σ_{BG}). (b) The variation of D for a variable background stress and constant background strain rate. (c) The dependence of D on the thermal conductivity. (d) The variation of D with the stress exponent n. (e and f) The sensitivity of D to E_A and T_0 are depicted. Thicknesses were evaluated at 25% shortening; crosses depict experiments that ran using a constant thermal conductivity, whereas the diamonds correspond to simulations utilizing temperature-dependent conductivity (see Table 1). Models with variables n, E_A, and T_0 were computed for a fixed background strain rate and stress; the preexponent factor A was hence varied accordingly. The solid black lines correspond the analytical scaling law described in section 3.

3. Results

3.1. Reference Model

The time evolution of the reference model is presented in Figures 1 and 2. Shear localization initiates from the stress perturbation generated by the inclusion (Figure 1a). The shear zones start to develop at $< 5\%$ bulk shortening. Up to $\approx 15\%$, the shear zones are in a strongly transient stage (Figure 2a). During that period the shear band narrows to reach a thickness of ≈ 2.5 km. Coevally, a temperature rise of $\approx 120°$C, and one-order of magnitude $\dot{\epsilon}_{II}$ amplification takes place within the shear zone (Figures 2c and 2d). Shear band rotation and advection occur during the $\approx 40\%$ shortening and is not affected by the transient stage (Figure 2b). This effect is the result of finite strain and records of the memory of the thermal weakening, which is inherent to thermomechanically coupled models.

According to the physical prediction of section 2.2, the thermomechanical models are controlled by physical parameters, excluding the dimension of the initial perturbation. Figure 3a shows the insensitivity of the reference model to the radius of the circular inclusion after 20% shortening. Although the size of the inclusion affects the transient stage of the inclusion [*Kaus and Podladchikov*, 2006], a variation of inclusion radius over 1 order of magnitude does not notably impact on the shear zone thickness, nor the strain rate amplitude, at large deformation.

Furthermore, since shear zone generation is only controlled by physical parameters, the models should exhibit essentially no dependence on the numerical resolution as long as the physical scales relevant for the physical processes are resolved. Figure 3b displays the model evolution for three different grid resolutions at 20% shortening. The three simulations exhibit a similar localization pattern and strain rate amplitude within

the shear zones which are essentially independent on the resolution. Similar mesh insensitive behavior of thermally activated shear localization was reported by *Takeuchi and Fialko* [2012].

3.2. Approximate Scaling Versus Numerical Results

Systematic numerical simulations were performed to validate the analytical prediction of section 2.2. Figure 4 shows the comparison of numerical results with the scaling law for variable controlling physical parameters. The scaling law was computed using a scaling coefficient K, equal to 30. For variations of either background strain rate (at constant background stress), background stress (at constant background strain rate), thermal conductivity, stress exponent, activation energy, or initial temperature, a good fit was obtained. This indicates that the proposed scaling law is a robust tool that allows to predict ductile shear zone thickness over a large range of geological parameters. Models taking into account temperature-dependent thermal conductivity were also performed, and we could show that such nonlinearity does not notably affect the scaling (Figures 4a and 4b).

4. Discussion

In numerous geodynamic numerical models of shear zone formation, weakening is caused by material softening (or strain softening). The application of strain softening causes mesh dependencies in shear zone modeling [*Bažant*, 1988] and hence non grid-convergent numerical solutions. Regularization techniques must be used to avoid the mesh dependency [*Bažant*, 1988; *de Borst and Sluys*, 1991; *de Borst and Mühlhaus*, 1992]. Application of a regularization means that a characteristic length scale is introduced in the governing equations, and this length scale controls the shear zone thickness. Hence, the shear zone thickness is defined a priori and is not controlled by the physics. The regularization therefore limits the predictive power of numerical simulations employing strain softening with respect to the shear zone thickness and hence with respect to magnitudes of stress, pressure, and temperature within the shear zone. Using a thermomechanical feedback, shear zones can develop spontaneously and have a finite width controlled by well-determined material parameters and far-field loading conditions. Shear localization due to viscous heating is presumably one of the simplest self-consistent models that provides a physics-controlled shear zone thickness in crustal rocks dominated by viscous deformation. For shallow crustal conditions and seismic slip rates, *Platt et al.* [2014] could also show that thickness of shear zones ($\mathcal{O}(10)$ μm) in fluid-saturated gauge is controlled by the physical properties of the material.

Our thermomechanical parameters and loading conditions are representative for the deformation of the continental crust. For stresses <1 GPa our model predicts shear zone thicknesses between ≈1 km and ≈7 km (Figure 4). These values are typical for ductile shear zones within the crust and lithosphere [*Davis*, 1983; *Cloos and Shreve*, 1996; *Pili et al.*, 1997] and are in agreement with the results of *Takeuchi and Fialko* [2012]. Moreover, such thicknesses correspond to the characteristic thickness of many tectonic nappes observed in the European Alps [*Steck*, 2008]. Many of these tectonic nappes are considered to be formed by ductile shear zones [*Steck*, 2008] which is supported by our shear zone thickness estimates for crustal conditions. The agreement between predicted shear zone thickness and observed shear zone thickness suggests that viscous heating was a controlling process during the formation of crustal and lithospheric shear zones, and of tectonic nappes. The predicted temperature increase for crustal conditions is between 50°C and 200°C. Such temperature rise seems feasible for natural crustal shear zone [*Camacho et al.*, 2001] and is in agreement with previous modeling results [*Takeuchi and Fialko*, 2012]. In addition to shear heating, viscous deformation may be assisted by grain size reduction [e.g., *Kameyama et al.*, 1997] or occur in an exponential flow regime. Both deformation mechanisms can yield to an increase of the effective stress exponent, further enhancing strain localization [*Montési and Zuber*, 2002; *Schmalholz and Fletcher*, 2011]. Such increase of the stress exponent will, according to our scaling law, results in smaller-scale shear zones. Additionally, mineral reactions [e.g., *Oliot et al.*, 2010] may as well act as a softening mechanism, which will further contribute to the long-term memory of the strained lithosphere.

5. Conclusions

Our results show that the thickness of ductile shear zones that are caused by viscous heating is controlled by thermomechanical material properties and far-field loading conditions. Numerical simulations show that the shear zone thickness is essentially independent on the numerical resolution and the size of the initial perturbation. The shear zone thickness can hence be predicted by a simple scaling law that includes parameters

that are not related to the shear zone (e.g., strain rate or stress inside the shear zone). For parameters that are typical for crustal deformation our model predicts shear zone thickness between 1 km and 7 km, which is in agreement with the thickness of natural crustal shear zones. Our results hence suggest that viscous heating is a controlling process during the formation of these crustal shear zones.

Acknowledgments
The data presented in this paper are the result of dimensional analysis (see section 2.2) and forward numerical simulations (see section 2.3). The authors thank Boris Kaus and an anonymous reviewer for providing insightful reviews. Dave Yuen thanks the CMG program of NSF. This work was supported by the University of Lausanne. For reproducibility reasons, additional information is available in the supporting information.

The Editor thanks Boris Kaus and an anonymous reviewer for their assistance in evaluating this paper.

References

Bažant, Z. (1988), Softening instability: Part I—Localization into a planar band, *J. Appl. Mech.*, *55*(3), 517–522.
Bird, P. (1978), Stress and temperature in subduction shear zones: Tonga and Mariana, *Geophys. J. Int.*, *55*(2), 411–434.
Braeck, S., and Y. Y. Podladchikov (2007), Spontaneous thermal runaway as an ultimate failure mechanism of materials, *Phys. Rev. Lett.*, *98*, 095504.
Brun, J., and P. Cobbold (1980), Strain heating and thermal softening in continental shear zones: A review, *J. Struct. Geol.*, *2*(1-2), 149–158.
Camacho, A., I. McDougall, R. Armstrong, and J. Braun (2001), Evidence for shear heating, Musgrave Block, central Australia, *J. Struct. Geol.*, *117*, 1007–1013.
Carter, N. L., and M. C. Tsenn (1987), Flow properties of continental lithosphere, *Tectonophysics*, *136*, 27–36.
Clauser, C., and E. Huenges (1995), Thermal conductivity of rocks and minerals, in *Rock Physics and Phase Relations*, edited by T. J. Ahrens, pp. 105–126, AGU, Washington, D. C.
Cloos, M., and R. Shreve (1996), Shear-zone thickness and the seismicity of Chilean- and Marianas-type subduction zones, *Geology*, *24*(2), 107–110.
Davis, G. (1983), Shear-zone model for the origin of metamorphic core complexes, *Geology*, *11*(6), 342–347.
de Borst, R., and H.-B. Mühlhaus (1992), Gradient-dependent plasticity: Formulation and algorithmic aspects, *Int. J. Numer. Methods Eng.*, *35*(3), 521–539.
de Borst, R., and L. Sluys (1991), Localisation in a cosserat continuum under static and dynamic loading conditions, *Comput. Methods Appl. Mech. Engng.*, *90*(1-3), 805–827.
Dodd, B., and Y. Bai (2012), *Adiabatic Shear Localization*, Frontiers and Advances, Elsevier, Amsterdam, Netherlands.
Duprat-Oualid, S., P. Yamato, and P. Pitra (2013), Major role of shear heating in intracontinental inverted metamorphism: Inference from a thermo-kinematic parametric study, *Tectonophysics*, *608*, 812–831.
Duretz, T., D. A. May, T. V. Gerya, and P. J. Tackley (2011), Discretization errors and free surface stabilization in the finite difference and marker-in-cell method for applied geodynamics: A numerical study, *Geochem. Geophys. Geosyst.*, *12*, Q07004, doi:10.1029/2011GC003567.
England, P., and P. Molnar (1993), The interpretation of inverted metamorphic isograds using simple physical calculations, *Tectonics*, *12*(1), 146–157.
Fleitout, L., and C. Froidevaux (1980), Thermal and mechanical evolution of shear zones, *J. Struct. Geol.*, *2*(1-2), 159–164.
Gerya, T. V. (2010), *Introduction to Numerical Geodynamic Modelling*, 345 pp., Cambridge Univ. Press, Cambridge, U. K.
Gibbons, W. (2008), Transcurrent ductile shear zones and the dispersal of the Avalon superterrane, in *The Cadomian Orogeny, Geol. Soc. Spec. Publ.*, *51*, 407–423.
John, T., S. Medvedev, L. H. Rupke, T. B. Andersen, Y. Y. Podladchikov, and H. Austrheim (2009), Generation of intermediate-depth earthquakes by self-localizing thermal runaway, *Nat. Geosci.*, *2*(2), 137–140.
Kameyama, M., D. A. Yuen, and H. Fujimoto (1997), The interaction of viscous heating with grain-size dependent rheology in the formation of localized slip zones, *Geophys. Res. Lett.*, *24*(20), 2523–2526.
Kaus, B. J. P., and Y. Y. Podladchikov (2006), Initiation of localized shear zones in viscoelastoplastic rocks, *J. Geophys. Res.*, *111*, B04412, doi:10.1029/2005JB003652.
Leloup, P. H., Y. Ricard, J. Battaglia, and R. Lacassin (1999), Shear heating in continental strike-slip shear zones: Model and field examples, *Geophys. J. Int.*, *136*(1), 19–40.
Minakov, A., Y. Podladchikov, J. Faleide, and R. Huismans (2013), Rifting assisted by shear heating and formation of the Lomonosov Ridge, *Earth Planet. Sci. Lett.*, *373*, 31–40.
Montési, L. G. J., and M. T. Zuber (2002), A unified description of localization for application to large-scale tectonics, *J. Geophys. Res.*, *107*(B3), ECV 1-1–ECV 1-21, doi:10.1029/2001JB000465.
Oliot, E., P. Goncalves, and D. Marquer (2010), Role of plagioclase and reaction softening in a metagranite shear zone at mid-crustal conditions (Gotthard Massif, Swiss Central Alps), *J. Metamorph. Geol.*, *28*(8), 849–871.
Pili, E., Y. Ricard, J.-M. Lardeaux, and S. Sheppard (1997), Lithospheric shear zones and mantle-crust connections, *Tectonophysics*, *280*(1-2), 15–29.
Platt, J. D., J. W. Rudnicki, and J. R. Rice (2014), Stability and localization of rapid shear in fluid-saturated fault gouge: 2. Localized zone width and strength evolution, *J. Geophys. Res. Solid Earth*, *119*, 4334–4359, doi:10.1002/2013JB010711.
Prieto, G. A., M. Florez, S. A. Barrett, G. C. Beroza, P. Pedraza, J. F. Blanco, and E. Poveda (2013), Seismic evidence for thermal runaway during intermediate-depth earthquake rupture, *Geophys. Res. Lett.*, *40*, 6064–6068, doi:10.1002/2013GL058109.
Ramsay, J. (1980), Shear zone geometry: A review, *J. Struct. Geol.*, *2*(1-2), 83–99.
Ranalli, G. (1995), *Rheology of the Earth,* 2nd ed., Chapman and Hall, London, U. K.
Regenauer-Lieb, K., and D. Yuen (2003), Modeling shear zones in geological and planetary sciences: Solid- and fluid-thermal mechanical approaches, *Earth Sci. Rev.*, *63*(3-4), 295–349.
Schmalholz, S. M., and R. C. Fletcher (2011), The exponential flow law applied to necking and folding of a ductile layer, *Geophys. J. Int.*, *184*(1), 83–89.
Schmalholz, S. M., and Y. Y. Podladchikov (2013), Tectonic overpressure in weak crustal-scale shear zones and implications for the exhumation of high-pressure rocks, *Geophys. Res. Lett.*, *40*, 1984–1988, doi:10.1002/grl.50417.
Steck, A. (2008), Tectonics of the Simplon massif and Lepontine gneiss dome: Deformation structures due to collision between the underthrusting European plate and the Adriatic indenter, *Swiss J. Geosci.*, *101*(2), 515–546.
Steck, A., F. Della Torre, F. Keller, H.-R. Pfeifer, J. Hunziker, and H. Masson (2013), Tectonics of the Lepontine Alps: Ductile thrusting and folding in the deepest tectonic levels of the Central Alps, *Swiss J. Geosci.*, *106*(3), 427–450.
Takeuchi, C. S., and Y. Fialko (2012), Dynamic models of interseismic deformation and stress transfer from plate motion to continental transform fault, *J. Geophys. Res.*, *117*, B05403, doi:10.1029/2011JB009056.
Thatcher, W., and P. C. England (1998), Ductile shear zones beneath strike-slip faults: Implications for the thermomechanics of the San Andreas Fault Zone, *J. Geophys. Res.*, *103*(B1), 891–905.

Thielmann, M., and B. J. Kaus (2012), Shear heating induced lithospheric-scale localization: Does it result in subduction?, *Earth Planet. Sci. Lett.*, *359-360*, 1–13.
Walley, S. (2007), Shear localization: A historical overview, *Metall. Mater. Trans. A*, *38*(11), 2629–2654.
Wernicke, B. (1985), Uniform-sense normal simple shear of the continental lithosphere, *Can. J. Earth Sci.*, *22*(1), 108–125.
Wright, T. M. (2002), *The Physics and Mathematics of Adiabatic Shear Bands*, Cambridge Monographs on Mechanics, Cambridge Univ. Press, Cambridge, U. K.
Yuen, D. A., L. Fleitout, G. Schubert, and C. Froidevaux (1978), Shear deformation zones along major transform faults and subducting slabs, *Geophys. J. R. Astron. Soc.*, *54*(1), 93–119.